RESEARCH ARTICLE

Structured and Dynamic Disordered Domains Regulate the Activity of a Multifunctional Anti-σ Factor

Julien Herrou,[a] Jonathan W. Willett,[a] Sean Crosson[a,b]

Department of Biochemistry and Molecular Biology, University of Chicago, Chicago, Illinois, USA[a]; The Committee on Microbiology, University of Chicago, Chicago, Illinois, USA[b]

ABSTRACT **The anti-σ factor NepR plays a central role in regulation of the general stress response (GSR) in alphaproteobacteria. This small protein has two known interaction partners: its cognate extracytoplasmic function (ECF) σ factor and the anti-anti-σ factor, PhyR. Stress-dependent phosphorylation of PhyR initiates a protein partner switch that promotes phospho-PhyR binding to NepR, which frees ECF σ to activate transcription of genes required for cell survival under adverse or fluctuating conditions. We have defined key functional roles for structured and intrinsically disordered domains of *Caulobacter crescentus* NepR in partner binding and activation of GSR transcription. We further demonstrate that NepR strongly stimulates the rate of PhyR phosphorylation *in vitro* and that this effect requires the structured and disordered domains of NepR. This result provides evidence for an additional layer of GSR regulation in which NepR directly influences activation of its binding partner, PhyR, as an anti-anti-σ factor. We conclude that structured and intrinsically disordered domains of NepR coordinately control multiple functions in the GSR signaling pathway, including core protein partner switch interactions and pathway activation by phosphorylation.**

IMPORTANCE **Anti-σ factors are key molecular participants in a range of adaptive responses in bacteria. The anti-σ factor NepR plays a vital role in a multiprotein partner switch that governs general stress response (GSR) transcription in alphaproteobacteria. We have defined conserved and unconserved features of NepR structure that determine its function as an anti-σ factor and uncovered a functional role for intrinsically disordered regions of NepR in partner binding events required for GSR activation. We further demonstrate a novel function for NepR as an enhancer of PhyR phosphorylation; this activity also requires the disordered domains of NepR. Our results provide evidence for a new layer of GSR regulatory control in which NepR directly modulates PhyR phosphorylation and, hence, activation of the GSR.**

Received 28 May 2015 **Accepted** 8 July 2015 **Published** 28 July 2015

Citation Herrou J, Willett JW, Crosson S. 2015. Structured and dynamic disordered domains regulate the activity of a multifunctional anti-σ factor. mBio 6(4):e00910-15. doi: 10.1128/mBio.00910-15.

Invited Editor Michael T. Laub, Massachusetts Institute of Technology **Editor** Dianne K. Newman, California Institute of Technology/HHMI

Address correspondence to Sean Crosson, scrosson@uchicago.edu.

J.H. and J.W.W. contributed equally to this article.

Cells employ numerous mechanisms to modulate gene expression in response to changes in the physical and chemical state of the environment. In bacteria, this process is commonly mediated by one of two mechanisms of transcriptional control: (i) two-component signal transduction (TCS) and (ii) alternative σ factor (σ) regulation. The alphaproteobacteria respond to multiple environmental stressors via an atypical, hybrid TCS-σ signaling pathway that controls activity of an extracytoplasmic function (ECF) σ factor, EcfG (1–3). σ^{EcfG} activity is regulated at the post-translational level by a partner switch mechanism involving its anti-σ factor, NepR, and the anti-anti-σ factor, PhyR (1). Briefly, phosphorylation of the C-terminal receiver domain of PhyR promotes NepR binding to the σ-like domain of PhyR (PhyR-SL) (4, 5); this frees σ^{EcfG} to associate with RNA polymerase (RNAP) and activate transcription (Fig. 1). PhyR, NepR, and σ^{EcfG} are broadly conserved in the class *Alphaproteobacteria* and have been demonstrated to regulate transcription and cell survival in the face of various environmental stressors (1, 6–16).

The primary EcfG family σ factor of *Caulobacter crescentus*, annotated σ^{T}, is a demonstrated regulator of transcription and cell survival under adverse growth conditions (11, 16, 17). The *C. crescentus* histidine kinase (HK) PhyK phosphorylates PhyR upon stress encounter (16), which promotes its association with NepR and releases σ^{T} to activate transcription (5, 16) (Fig. 1A). *C. crescentus* NepR contains two highly conserved central helices (α1 and α2) connected by a short, 4-residue linker (5). Poorly conserved regions of primary structure (see Fig. S1A in the supplemental material) that we term flanking regions 1 (FR1) and 2 (FR2) border α1 and α2, respectively (2) (Fig. 1C). High-resolution structures of PhyR-SL in complex with NepR determined by X-ray crystallography (5) and nuclear magnetic resonance (NMR) spectroscopy (4) support a model in which NepR α1-α2 is the main structural element that interacts with PhyR-SL (Fig. 1B). These experimental structural data also provide evidence that FR1 and FR2 termini are dynamic and disordered (see Fig. S1B). Though the dynamic termini have highly divergent primary structures, there is evidence that FR1 is required for proper NepR function as an anti-σ^{EcfG} factor in *Sinorhizobium meliloti* (7). However, the

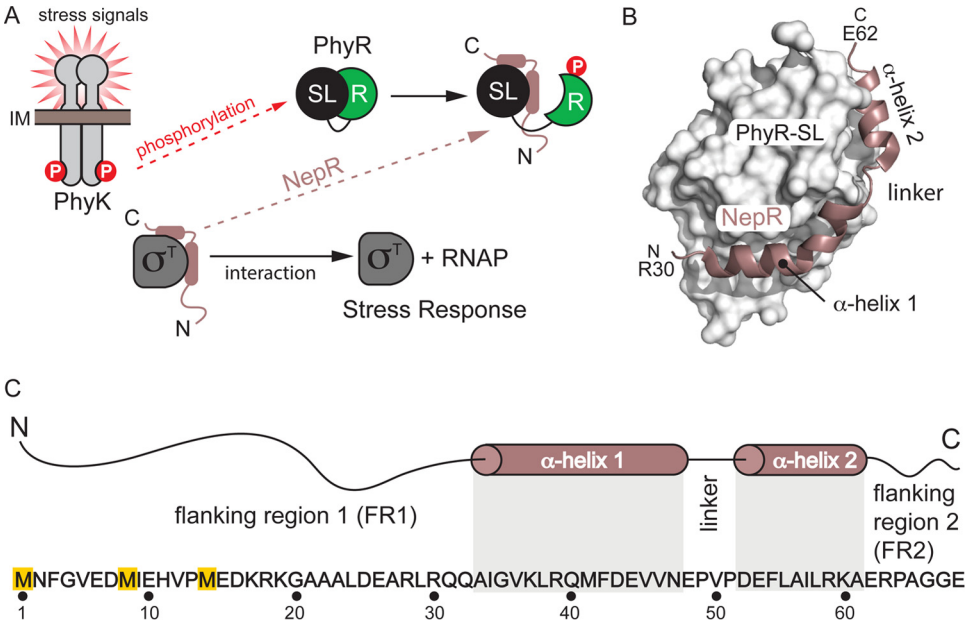

FIG 1 Model of the general stress response (GSR) system of alphaproteobacteria, including defined molecular components of *C. crescentus* GSR. (A) Under normal growth conditions, the ECF σ factor, σ^T, is bound and inhibited by the anti-σ factor NepR. Upon stress encounter, the sensor histidine kinase, PhyK, is proposed to phosphorylate PhyR, thereby increasing its affinity for NepR and releasing σ^T to bind RNAP. IM, inner membrane. (B) Surface representation of the structure of the σ-like domain of PhyR (PhyR-SL) (in white; M1 to E138) bound to NepR (in dark pink; R30 to E62) (PDB code 3T0Y) (5). (C) Amino acid sequence and secondary structure of *C. crescentus* NepR: N-terminal flanking region (FR1; M1 to Q32), α-helix 1 (α1; A33 to N47), linker (L; E48 to P51), α-helix 2 (α2; D52 to A61), and C-terminal flanking region (FR2; E62 to E68). Three putative NepR start codons are highlighted in yellow.

function(s) of the unconserved and disordered terminal regions of NepR remains largely uncharacterized.

Here, we delineate conserved and unconserved features of NepR structure that determine its function as an anti-σ factor. As in related species (4), the unconserved termini (FR1 and FR2) of *C. crescentus* NepR have primary structures that are consistent with an intrinsically disordered polypeptide. FR1 and FR2 are not required for NepR binding to the σ-like domain of PhyR (PhyR-SL) or to σ^T. The conserved central helical domain (α1-linker-α2) determines high-affinity binding between NepR and these substrates. However, NepR lacking FR1 fails to bind to full-length phospho-PhyR (PhyR~P) and does not function as an anti-σ factor *in vivo*. Thus, in the context of a fully intact general stress response (GSR) regulatory system in *C. crescentus* cells, NepR function requires both its conserved central helical domain and unconserved, disordered amino-terminal domain.

Our studies of NepR structure and function further reveal that this protein can also act to stimulate phosphorylation of its anti-anti-σ binding partner, PhyR. Specifically, NepR strongly enhances the rate of PhyR phosphorylation and increases steady-state levels of PhyR~P *in vitro*; this stimulatory activity requires full-length NepR protein, including the FR1 and FR2 regions. Our data thus provide evidence for an additional layer of GSR control in which low-affinity interaction of full-length NepR with unphosphorylated PhyR functions to enhance phosphorylation of the PhyR receiver domain and subsequent activation of GSR transcription. Our data support a model for NepR as a multifunctional anti-σ factor composed of two functionally distinct regions: (i) a central helical domain that forms an ordered three-dimensional structure and directly interacts with ECF σ and the σ-like domain of PhyR and (ii) an intrinsically disordered amino terminus that determines stable binding to full-length PhyR and ECF σ and that is required for stimulation of PhyR receiver domain phosphorylation.

RESULTS

Unconserved and conserved domains govern NepR binding to full-length PhyR. Ribosome profiling of the 5′ region of *nepR* revealed three possible start codons (18), suggesting that *nepR* translation could initiate from multiple sites to yield different isoforms. We show that translation of *nepR* is highest when all three start codons are present (see Fig. S2 in the supplemental material). To test whether these different putative isoforms of NepR may differentially interact with PhyR and σ^T, we used a bacterial two-hybrid (BTH) protein interaction system (19). Three alleles of *nepR* starting at each of the putative translation start sites (codon 1-$NepR_{FL}$ [full length], codon 8-$NepR_{SC2}$ [start codon 2], and codon 14-$NepR_{SC3}$ [start codon 3]) were fused to the T18 fragment and transformed into an *Escherichia coli* reporter strain expressing full-length PhyR (*phyR*), PhyR-SL (*phyR-SL*), or σ^T (*sigT*) fused to T25. Serial truncation of the first 13 residues of NepR does not have a statistically significant effect on binding to PhyR, PhyR-SL, or σ^T (Fig. 2). Thus, all three versions of NepR are functional in a BTH assay, insofar as they interact with full-length PhyR, PhyR-SL, and σ^T.

The observed interactions between full-length PhyR and alleles of NepR by BTH assay suggest that PhyR is phosphorylated in the *E. coli* cytoplasm, as strong PhyR-NepR binding is dependent on phosphorylation of the PhyR receiver domain (1, 5, 16). To test this hypothesis, we generated T25-PhyR with a mutation in the conserved aspartyl phosphorylation site (D192) of the PhyR receiver domain. No interaction between $PhyR_{D192A}$ and NepR was

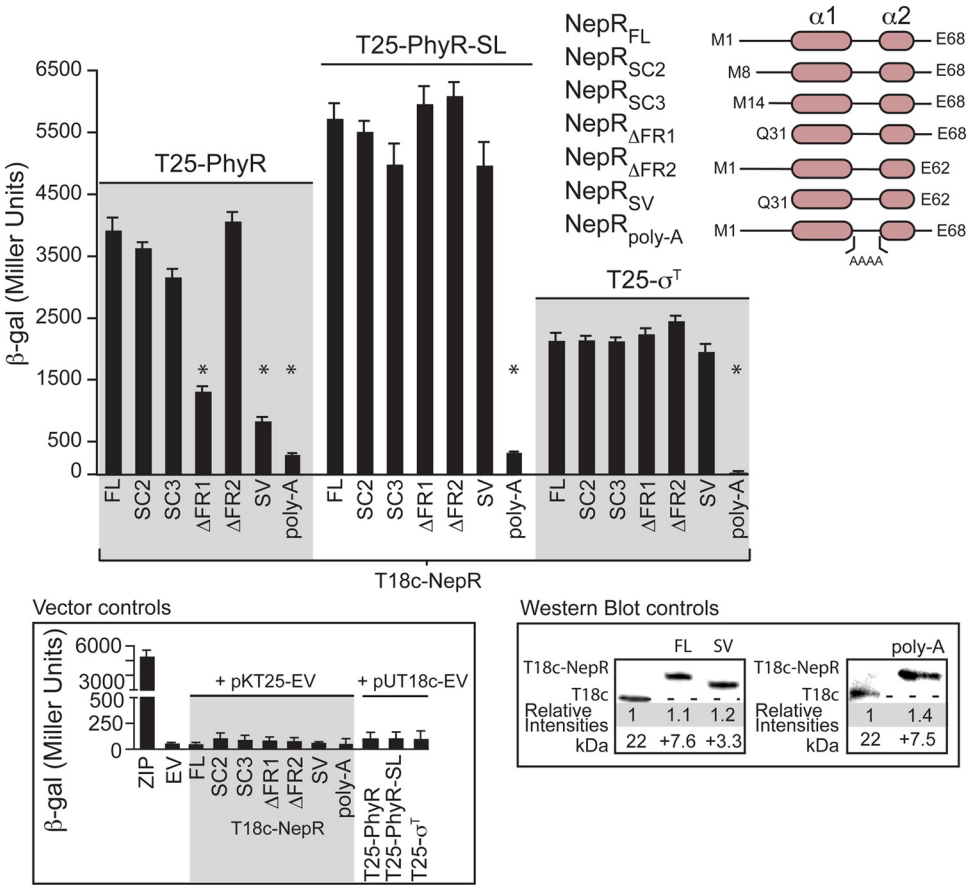

FIG 2 Interaction of full-length and mutant NepR alleles with PhyR, PhyR σ-like domain (PhyR-SL), and σ^T assessed by bacterial two-hybrid (BTH) assay. (Top right) Cartoon representation of the full-length (FL), truncated, and site-directed NepR mutant alleles assayed for interaction with σ^T, PhyR, and PhyR-SL. (Middle) Protein interaction results reported as β-galactosidase activity, measured in BTH reporter strains transformed with pUT18c expressing *nepR* alleles pictured on top right: full length (FL; M1 to E68), start codon 2 (SC2; M8 to E68), start codon 3 (SC3; M14 to E68), flanking region 1 deleted (ΔFR1; Q31 to E68), flanking region 2 deleted (ΔFR2; M1 to E62), short version (SV; Q31 to E62), and polyalanine linker (poly-A); each of these NepR alleles was measured for interaction with PhyR, PhyR-SL, or σ^T expressed from pKT25. (Bottom left) Positive (leucine zipper vectors), negative (empty vectors, EV), and vector controls. All assays were performed in triplicate; error bars represent standard deviations. (Bottom right) Stability of NepR alleles expressed in the BTH reporter strain was assessed by Western blotting using T18 antiserum.

observed in this strain (see Fig. S3A in the supplemental material), supporting the hypothesis that PhyR is phosphorylated in the *E. coli* reporter strain BTH101. Phosphorylation may be occurring through spurious interaction with an *E. coli* histidine kinase or by a low-molecular-weight phosphoryl donor, such as acetyl phosphate (AcP) (20).

The NepR N and C termini (FR1 and FR2, respectively) are dynamic (4) and disordered (4, 5) in experimental structures of NepR bound to PhyR-SL and display low sequence conservation across species (see Fig. S1A in the supplemental material) (5). Indeed, neural network algorithms (21, 22) trained on a known set of ordered and disordered structures in the Protein Data Bank (PDB) predict that FR1 and FR2 have properties of intrinsically disordered polypeptides (see Fig. S1B). To extend our structure-function analysis of these unconserved, disordered regions of NepR, we generated three additional truncated alleles: $nepR_{\Delta FR1}$ (expressing residues Q31 to E68), $nepR_{\Delta FR2}$ (expressing residues M1 to E62), and $nepR_{SV}$ (SV, short version; expressing residues Q31 to E62). These *nepR* alleles were fused to T18 and transformed into reporter strains expressing full-length PhyR, PhyR-SL, or σ^T fused to T25. Deletion of the disordered N and C termini of NepR does not affect binding to the isolated PhyR-SL domain or to σ^T via BTH assay (Fig. 2). However, deletion of the first 30 residues (FR1) of the NepR amino terminus results in a significant ($P < 0.01$) reduction in PhyR binding (Fig. 2). $NepR_{SV}$ (in which both FR1 and FR2 are deleted) has further-reduced binding to PhyR ($P < 0.01$). To further control these BTH interaction studies, we conducted the "reverse" experiment, in which each allele under investigation was reciprocally fused to either T25 or T18. No differences in interaction were observed when alleles were expressed from the reciprocal plasmid (see Fig. S3B). As an additional control, we confirmed that the proximity of the T18 subunit to $NepR_{SV}$ does not interfere with T25-PhyR interaction by adding a 30-amino-acid (aa) linker between T18 and $NepR_{SV}$. We observed an equivalently weak interaction between $NepR_{SV}$ and PhyR in this strain (see Fig. S3B).

Finally, we tested the function of the 4-residue linker sequence between NepR α1 and α2 in NepR substrate binding (Fig. 1C). This region of NepR forms extensive polar contacts with the σ-like (SL) domain of *C. crescentus* PhyR (5), suggesting that it plays an important role in PhyR-NepR interaction. A NepR allele with the linker sequence mutated to polyalanine (T18c-$NepR_{poly\text{-}A}$) does

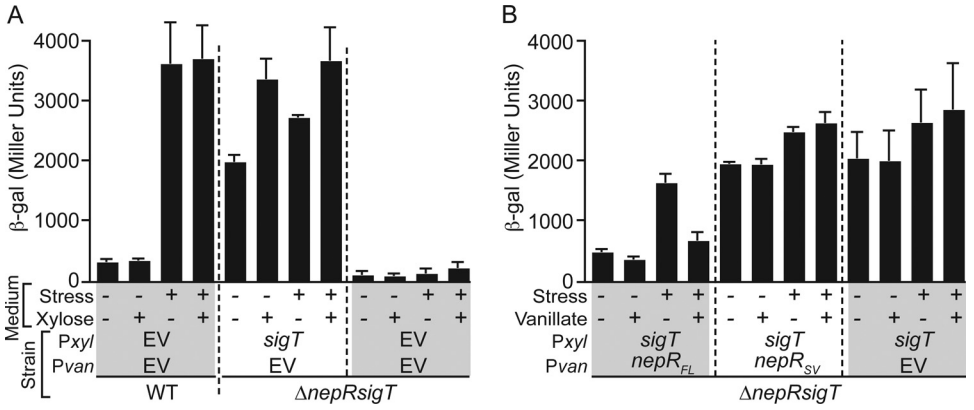

FIG 3 Functional analysis of full-length and truncated NepR alleles as regulators of GSR transcription in *C. crescentus*. (A) Measured β-galactosidase activity from the σ^T-dependent P_{sigU}-*lacZ* reporter plasmid. β-Galactosidase activities were measured in WT and Δ*nepR* Δ*sigT* backgrounds containing a plasmid expressing *sigT* from a xylose-inducible promoter (P_{xyl}-*sigT*), in the presence (+) or absence (−) of *sigT* inducer (0.2% xylose) and the presence (+) or absence (−) of osmotic upshock stress (150 mM sucrose). Empty vector (EV) controls (P_{xyl} and P_{van}) are also included. (B) σ^T-dependent transcription measured in a Δ*nepR* Δ*sigT* strain expressing *sigT* from P_{xyl}-*sigT*. Transcription was assayed as a function of full-length ($nepR_{FL}$) and terminally truncated ($nepR_{SV}$) *nepR* alleles expressed from a vanillate-inducible promoter (P_{van}-$nepR_{FL}$ or P_{van}-$nepR_{SV}$). Boundaries of expressed *nepR* alleles are as follows: $nepR_{FL}$, M1 to E68; $nepR_{SV}$, Q31 to E62. β-Galactosidase activities were assayed in the presence (+) and absence (−) of *nepR* induction (0.5 mM vanillate) and in the presence (+) and absence (−) of osmotic upshock (150 mM sucrose). Transcription was compared to an empty vector (EV) control strain. Stability and function of HA-tagged *nepR* alleles were further evaluated by dot blotting and β-galactosidase transcriptional assays described in Fig. S4 in the supplemental material. All assays were performed in triplicate; error bars represent standard deviations.

not interact with PhyR, PhyR-SL, or σ^T in our BTH assay, confirming the importance of this short linker sequence in the interaction of NepR with its substrates (Fig. 2). Western blot controls confirm that reduced PhyR binding to the $NepR_{SV}$ and $NepR_{poly\text{-}A}$ NepR alleles is not a function of variable concentrations of these fusion proteins in the cell (Fig. 2).

Disordered termini are required for NepR anti-σ function *in vivo*. We next sought to assess the functional implications of our two-hybrid interaction data (Fig. 2) using GSR-dependent transcription in *C. crescentus* cells as a functional readout. We first attempted to generate a strain of *C. crescentus* in which the chromosomal copy of *nepR* was deleted. We were unable to delete *nepR* alone but were able to simultaneously delete *nepR* and *sigT*. Similar results have been described in *Sphingomonas* species (14) and in *Sinorhizobium meliloti*, where *nepR* could not be deleted unless its cognate *ecfG* was first deleted (23). We successfully transformed the *C. crescentus* Δ*nepR* Δ*sigT* double deletion mutant with a xylose-inducible allele of *sigT* (P_{xyl}-*sigT*) and an empty plasmid containing the vanillate-inducible promoter (P_{van}), which enabled us to assess σ^T-dependent transcription as a function of induced σ^T expression (Fig. 3A).

In the absence of xylose, this strain had high constitutive transcription from a σ^T-dependent transcriptional reporter (P_{sigU}-*lacZ*) compared to an unstressed wild-type (WT) control strain (Fig. 3A), suggesting that there is leaky transcription of *sigT* from P_{xyl}. Induction of *sigT* expression by addition of 10 mM (0.15% [wt/vol]) xylose increased σ^T-dependent transcription. As expected, osmotic upshock stress (150 mM sucrose) did not have a significant effect on σ^T-dependent transcription in this background (Fig. 3A), as NepR is missing. As a negative control, we transformed the Δ*nepR* Δ*sigT* strain with empty plasmids containing P_{xyl} and P_{van} promoters (EV); we did not observe σ^T-dependent transcription in this strain under any condition (Fig. 3A).

We next evaluated the function of different *nepR* alleles as anti-σ^T factors in *C. crescentus*. Using a vanillate-inducible expression system (P_{van}), we confirmed that full-length *nepR* ($nepR_{FL}$) represses σ^T-dependent transcription in the Δ*nepR* Δ*sigT*/P_{xyl}-*sigT* strain (Fig. 3B). Leaky expression of $NepR_{FL}$ from P_{van} is also evident in this strain: we observed repression of σ^T-dependent transcription in either the presence or the absence of 0.5 mM vanillate. This dual induction strain responded normally to osmotic upshock, demonstrating that *sigT* and *nepR* expressed from separate plasmids are functional in a cellular context (Fig. 3B). Induction of *nepR* expression by addition of 0.5 mM vanillate repressed σ^T-dependent transcription under osmotic upshock stress conditions (Fig. 3B).

Using this dual *nepR-sigT* induction system, we next investigated the functional role of the unconserved, disordered termini (FR1 and FR2) in NepR function as an anti-σ^T factor. We transformed the Δ*nepR* Δ*sigT*/P_{xyl}-*sigT* strain with P_{van}-$nepR_{SV}$, which encodes NepR residues Q31 to E62. This central helical region of NepR structure binds the *C. crescentus* PhyR-SL domain (5) and interacts with σ^T by BTH (Fig. 2). However, expression of $nepR_{SV}$ does not inhibit σ^T-dependent transcription in *C. crescentus* (Fig. 3B). We were unable to generate a reagent that directly detects NepR in *C. crescentus* lysate. We thus constructed N- and C-terminally HA-tagged alleles of $nepR_{FL}$ *and* $nepR_{SV}$. While this is an imperfect approach to assess stability of untagged NepR alleles, Western dot blotting experiments provide evidence that $nepR_{SV}$ is expressed at approximately the same level as $nepR_{FL}$ in cells, though levels of these small polypeptides are variable across five independent replicates (see Fig. S4A in the supplemental material). We further show that $NepR_{SV}$ HA-tagged at either its N or C terminus also fails to function as an anti-σ factor in our cellular transcription assay while HA-tagged $NepR_{FL}$ still has the capacity to repress GSR transcription (see Fig. S4B). These results provide evidence that $NepR_{SV}$ does not have anti-σ^T function in *C. crescentus*, which is inconsistent with our two-hybrid interaction data

TABLE 1 Microscopic association (K_a) and dissociation (K_d) and calculated equilibrium (K_D) affinities of PhyR binding to full-length NepR ($NepR_{FL}$) and the short version of NepR missing FR1 and FR2 ($NepR_{SV}$)

	MBP-$NepR_{FL}$			MBP-$NepR_{SV}$		
PhyR	K_a, $(1/M \cdot s) \times 10^5$	K_d, $(1/s) \times 10^{-1}$	K_D, nM	K_a, $(1/M \cdot s) \times 10^5$	K_d, $(1/s) \times 10^{-1}$	K_D, nM
His-PhyR-SL	5.08 ± 1.78	1.1 ± 0.16	191 ± 7	4.65 ± 0.98	2.08 ± 0.26	455 ± 54
His-PhyR~P	1.34 ± 0.15	0.97 ± 0.31	744 ± 289	ND[a]	ND	ND

[a] ND, not determined.

in a heterologous system (Fig. 2). The implications of this finding are discussed below.

The dynamic, disordered NepR termini are required for binding to PhyR~P *in vitro*. The unconserved termini of NepR are required for strong binding to full-length PhyR in a BTH assay (Fig. 2) and for proper σ^T-dependent regulation of transcription in *C. crescentus* (Fig. 3B). However, BTH assays demonstrate that the termini of NepR are largely dispensable for binding to either the σ-like domain of PhyR (PhyR-SL) or σ^T (Fig. 2). As BTH assays may lack the sensitivity to quantify small changes in protein interactions, we used surface plasmon resonance (SPR) to more accurately quantify NepR interaction with PhyR. We measured the association and dissociation rate constants (k_{on} and k_{off}) of $NepR_{FL}$ and $NepR_{SV}$ binding to PhyR and PhyR-SL. NepR proteins were prepared as fusions to maltose-binding protein (MBP), while PhyR proteins were prepared as His tag fusions.

The equilibrium affinity of $NepR_{FL}$ for PhyR-SL calculated from the measured rate constants was 191 ± 7 nM (Table 1; see also Fig. S5A in the supplemental material), which is in agreement with previously reported measurements (5). Removal of the termini from NepR decreases its equilibrium affinity for PhyR-SL to 455 ± 54 nM (Table 1; see Fig. S5B). Thus, removal of the NepR termini clearly compromises binding to PhyR-SL, even though we observed $NepR_{SV}$–PhyR-SL interaction in our BTH assay (Fig. 2). The measured equilibrium affinity of full-length NepR ($NepR_{FL}$) for phospho-PhyR (PhyR~P) is 744 ± 289 nM (Table 1; see Fig. S5C). We were unable to detect binding between $NepR_{SV}$ and full-length PhyR~P by SPR (see Fig. S5D); no binding was detected between PhyR or PhyR-SL and an MBP control sample (see Fig. S5E and F). The SPR data are consistent with our BTH interaction data (Fig. 2) and provide additional experimental support for a model in which the unconserved NepR termini play a key functional role in binding to full-length PhyR~P. We were unable to quantify σ^T binding to NepR, due to our inability to purify isolated, soluble σ^T. Like *ecfG* family σ factors from other systems (1, 7, 9, 14), *C. crescentus* σ^T is largely insoluble when expressed in isolation in a heterologous system; our attempts to solubilize and refold σ^T inclusion bodies were unsuccessful.

NepR termini stabilize the anti-σ/ECF σ complex. Coexpression of His-σ^T with untagged $NepR_{FL}$ or $NepR_{SV}$ enabled purification of soluble σ^T/$NepR_{FL}$ and σ^T/$NepR_{SV}$ complexes by affinity chromatography (Fig. 4A). We further purified these soluble complexes by size exclusion chromatography (see Fig. S6A in the supplemental material). The difference in size of the two proteins in these complexes and the diffuse resolution and gel staining of the 3.6-kDa (32-amino-acid [aa]) $NepR_{SV}$ peptide made it difficult to draw conclusions about complex stoichiometry. As such, we coexpressed and copurified His-tagged σ^T bound to MBP-tagged NepR alleles; Coomassie blue staining of the two resolved fusion proteins in these complexes provides evidence that σ^T/$NepR_{FL}$ and σ^T/$NepR_{SV}$ purify at a 1:1 ratio (Fig. 4B; see also Fig. S6B). Although both NepR alleles interact with σ^T in these copurification assays, size exclusion chromatography-purified σ^T/$NepR_{SV}$ complex has a lower helical content and a lower melting temperature (T_m = 51.3 ± 0.5°C) than σ^T/$NepR_{FL}$ (T_m = 53.9 ± 0.6°C) as assessed by a circular dichroism (CD) thermal denaturation assay (Fig. 4C and D). To direct transcription, ECF σ factors undergo a conformational transition from a closed state to an open state, in which σ can bind RNA polymerase and contact the −35 and −10 boxes in the promoter region (24). Reduced folded stability of the σ^T/$NepR_{SV}$ complex is consistent with a model in which full-length NepR stabilizes the closed, inactive conformation of σ^T to a greater extent than does $NepR_{SV}$ (Fig. 3B). We acknowledge that the difference in folded stability between these two σ/anti-σ complexes is relatively small; a more complete explanation of the inability of $NepR_{SV}$ to fully stabilize σ^T in its closed, inactive form will likely require a better understanding of concentrations and affinities of competing σ factors and solvent conditions in the cell during stress (25).

NepR-dependent enhancement of PhyR phosphorylation requires the unconserved NepR termini. Studies of the response regulators (RRs) DrrB and CheY have demonstrated that substrate binding or the presence of additional domains adjacent to the receiver domain can impact RR phosphorylation (26, 27), and it has been reported previously that NepR can affect PhyR phosphorylation (28). We sought to quantify the effect of NepR binding on phosphorylation of the anti-anti-σ factor PhyR. *In vitro* phosphorylation of PhyR with its cognate histidine kinase, PhyK, has proven unsuccessful due to difficulty in purifying an active form of this kinase (16). As an alternative approach, we incubated PhyR with the high-energy phosphodonor acetyl phosphate (AcP), which is known to phosphorylate many bacterial RRs and has been successfully used as a proxy for phosphorylation of RRs by their cognate kinase (29). PhyR is phosphorylated at a low level in the presence of [^{32}P]AcP. Addition of equimolar (10 μM) MBP-$NepR_{FL}$ strongly enhances the phosphorylation rate and steady-state PhyR~P level in this assay, suggesting that NepR can function to control PhyR phosphorylation (Fig. 5A). Addition of equimolar (10 μM) MBP-$NepR_{SV}$ only weakly enhanced production of PhyR~P, demonstrating that the unconserved, disordered termini (FR1 and FR2) are required for full NepR-dependent activation of PhyR phosphorylation. Mutation of the conserved site of PhyR aspartyl phosphorylation to alanine ($PhyR_{D192A}$) prevented PhyR phosphorylation in either the presence or the absence of NepR (Fig. 5A).

We considered two biochemical models for the observed increase in steady-state PhyR~P levels *in vitro*: (i) NepR stabilizes the phosphoryl group on PhyR~P or (ii) NepR binding enhances PhyR phosphorylation by AcP. To test these two models, we first measured the half-life of phosphoryl loss from PhyR~P alone, and

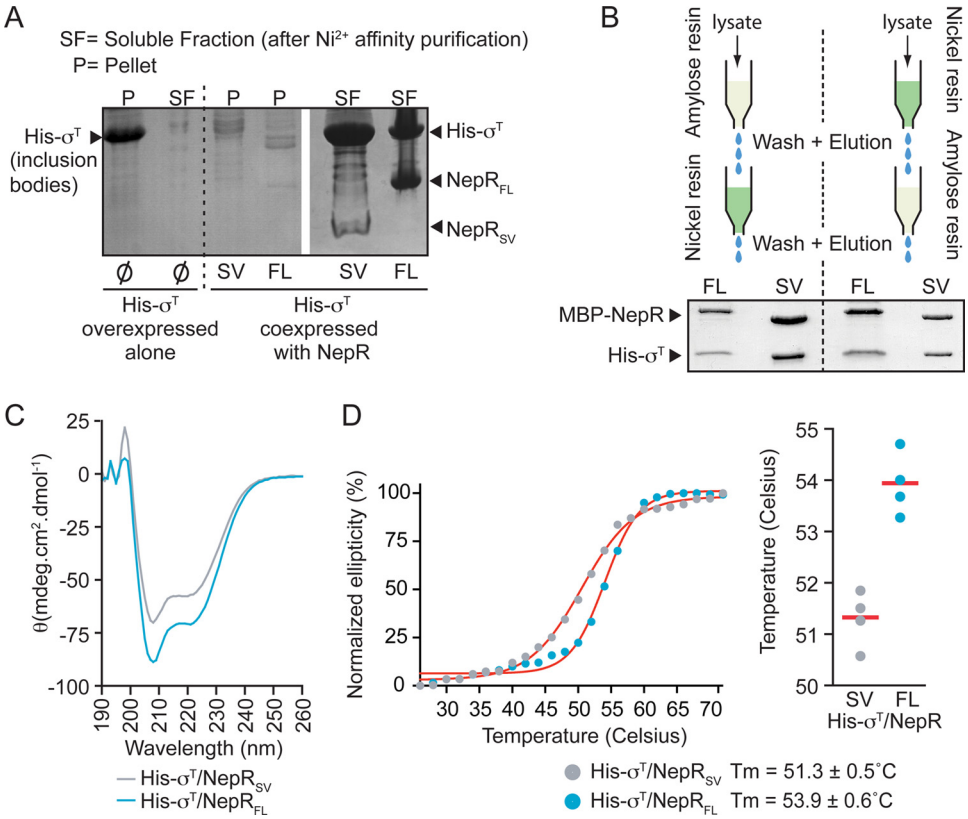

FIG 4 Measuring the effect of NepR termini on σ/anti-σ complex folded stability. (A) Expression and affinity purification of His-σ^T in presence or absence of $NepR_{FL}$ or $NepR_{SV}$. When overexpressed in isolation, His-σ^T is in the insoluble cell fraction (pellet [P]); no protein was retrieved from the soluble fraction (SF) after Ni^{2+} affinity chromatography (lane 2). When coexpressed with untagged $NepR_{FL}$ or $NepR_{SV}$, no His-σ^T is evident in the insoluble pellet fraction (P; lanes 3 and 4). The protein purifies as a σ^T/NepR (σ/anti-σ) complex in the soluble fraction (SF; lanes 5 and 6). (B) His-σ^T was coexpressed with MBP-NepR alleles. The complexes were sequentially purified by nickel and amylose affinity chromatographies and vice versa. Resolved proteins were visualized by Coomassie blue staining and support 1:1 binding for $\sigma^T/NepR_{FL}$ and $\sigma^T/NepR_{SV}$. (C) Circular dichroism (CD) spectra of $\sigma^T/NepR_{FL}$ and $\sigma^T/NepR_{SV}$ complexes at 26°C. (D) (Left) Representative normalized CD thermal denaturation trace of the $\sigma^T/NepR_{FL}$ and $\sigma^T/NepR_{SV}$ complexes; molar ellipticity at 222 nm was normalized by setting the value at 26°C to 0% and the value at 72°C to 100%. Change in ellipticity at 222 nm (3 acquisitions every 2°C) was plotted and fitted according to a Boltzmann model. (Right) Melting temperatures were measured four times on independent protein preparations. The horizontal bar represents the mean of all four measures. His-σ^T/MBP control and gel filtration elution profiles of the different complexes used for CD T_m are presented in Fig. S6 in the supplemental material.

in the presence of equimolar MBP, MBP-$NepR_{FL}$, and MBP-$NepR_{SV}$. The half-life of PhyR~P is ~47 h in the absence of NepR and ~49 h in the presence of NepR (Table 2), indicating that NepR does not significantly enhance the stability of PhyR~P. To test whether NepR stimulates PhyR phosphorylation, we incubated PhyR with AcP (in the presence and absence of $NepR_{FL}$ and $NepR_{SV}$) and measured the increase of PhyR~P as a function of time. Considering PhyR phosphorylation as a first-order process, we observe an approximately 50-fold increase in the apparent rate of PhyR phosphorylation in the presence of $NepR_{FL}$ compared to PhyR alone (Fig. 5B). $NepR_{SV}$ has only a weak stimulatory effect on PhyR phosphorylation; the level of measured PhyR~P after a 750-min incubation is 30% of that for $NepR_{FL}$ (Fig. 5B). We conclude that the stimulatory effect of NepR on the rate of PhyR phosphorylation requires one or both of the unconserved NepR termini. It remains to be determined if NepR promotes PhyK-dependent phosphorylation of PhyR *in vivo*.

DISCUSSION

The anti-σ factor NepR plays a key role in regulation of the general stress response in alphaproteobacteria (1, 2). Structures of NepR bound to the σ-like domain of PhyR (PhyR-SL) (4, 5) revealed two conserved central helices (α1 and α2) composed of approximately 30 residues that interact with PhyR-SL (Fig. 1B). A four-residue linker between α1 and α2 plays a critical functional role in NepR binding to σ^T, PhyR, and PhyR-SL. The N and C termini of NepR (FR1 and FR2, respectively) are poorly conserved (2), dynamic, and disordered and do not evidently interact with PhyR-SL in these structures (4, 5). Nonetheless, *nepR* orthologs across the class *Alphaproteobacteria* invariably contain unconserved, disordered extensions that flank the conserved central helical domain. This raised the question of what role, if any, these flanking regions have in NepR function as an anti-σ factor.

NepR FR1 and FR2 are not required for binding to σ^T or PhyR-SL but are necessary to bind full-length phospho-PhyR (PhyR~P) (Fig. 2; Table 1; see also Fig. S5 in the supplemental material). Biophysical analysis of purified σ^T/NepR complexes provides evidence that FR1 and FR2 increase the folded stability of the σ^T/NepR complex (Fig. 4), supporting a model in which the dynamic and disordered NepR termini function to stabilize the "closed" inhibited form of σ^T. Indeed, our *in vivo* studies of the

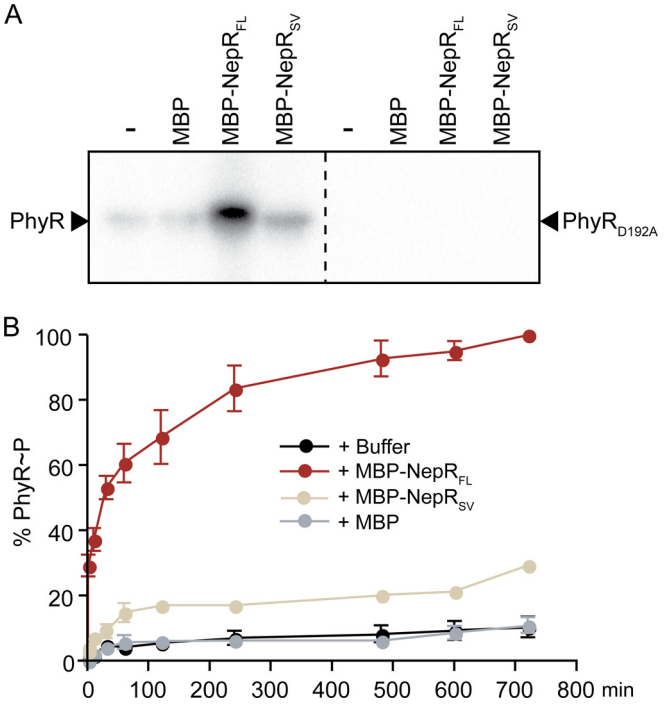

FIG 5 Acetyl phosphate (AcP)-dependent phosphorylation of PhyR requires NepR and PhyR residue D192. (A) Radiograph showing phosphorylation of PhyR (left) and PhyR$_{D192A}$ (right) by [^{32}P]AcP in the presence or absence of equivalent concentrations of MBP, MBP-NepR$_{FL}$, or MBP-NepR$_{SV}$ after a 120-min incubation. (B) Kinetics of AcP-dependent phosphorylation of PhyR alone or incubated with equimolar amounts (10 μM) of MBP, MBP-NepR$_{FL}$, or MBP-NepR$_{SV}$. Time is shown in minutes; the maximum level of PhyR phosphorylation observed was set to 100%. All experiments were performed in triplicate; error bars represent standard deviations.

C. crescentus regulatory system provide evidence that the intrinsically disordered terminal domains are necessary for NepR function as an anti-σ^T factor in the cell (Fig. 3). In brief, the central α1-α2 helical domain of NepR is not sufficient to function as a regulated anti-σ factor on its own even though it is competent to bind both σ (σ^T) and anti-anti-σ (PhyR-SL) substrates. The unconserved, dynamic, and disordered NepR amino terminus plays an indispensable role in binding of the central helical domain to its substrates in the context of the fully intact regulatory system. The structural basis by which intrinsically disordered regions enable NepR function as a regulated anti-σ factor is an open area of investigation. Certainly, we cannot exclude the possibility that FR1 and FR2 are ordered and structured when interacting with full-length PhyR~P or σ^T. Indeed, NMR studies of the orthologous system in *Sphingomonas* species demonstrate that NepR undergoes a disorder-order transition when binding PhyR-SL (4), although the structural states of FR1 and FR2 when bound to full-length PhyR or σ^T remain undefined.

Our study has also detailed a biochemical function of NepR as a protein that enhances the rate of PhyR phosphorylation and steady-state phospho-PhyR levels *in vitro* (Fig. 5). Our observation that NepR promotes PhyR phosphorylation (Fig. 5) appears to conflict with an apparent lack of stable association between unphosphorylated PhyR and NepR (Table 1). It may be that weak or transient PhyR-NepR interaction, below the detection limit of our methods, promotes phosphorylation of PhyR. In such a model, transient NepR interaction with unphosphorylated PhyR may "prime" PhyR for phosphorylation and subsequent high-affinity binding to NepR. Alternatively, it is possible that the PhyR-NepR interaction *in vivo* is chaperoned by another protein(s) (e.g., the PhyR kinase, PhyK). It remains to be determined if NepR promotes kinase-dependent phosphorylation of PhyR in the *C. crescentus* cell. Nonetheless, our results are consistent with a recent observation that the presence of NepR improves phosphorylation of *Sphingomonas melonis* PhyR by cognate kinases (28). Thus, NepR-dependent enhancement of PhyR phosphorylation may be a general feature of GSR regulation in alphaproteobacteria.

Our data provide an interesting example of a two-component receiver domain that is allosterically regulated by interaction with a nonkinase binding partner. Thus, there are biochemical regulatory parallels between the NepR-PhyR general stress system of alphaproteobacteria and the *E. coli* chemotaxis system, in which the CheY receiver phosphorylation rate is enhanced by CheZ or FliM binding (26, 27). Though the structural mechanism of NepR activity as an enhancer of PhyR phosphorylation remains undefined, we show that this activity requires one or both of the unconserved NepR termini. The FR1/FR2 termini of NepR may affect the structure of the PhyR receiver phosphorylation site, thereby enhancing phosphorylation by AcP. We note that the observed requirement of the NepR termini for this activity may be an indirect result of weaker binding of truncated NepR to PhyR. Regardless, this result solidifies the functional importance of unconserved, intrinsically disordered regions in multiple activities of this anti-σ factor. In conclusion, our study provides evidence that the anti-σ factor NepR coordinately utilizes structured and intrinsically disordered domains to control multiple functions in the alphaproteobacterial GSR, including repression of σ^T transcriptional activity and anti-anti-σ (i.e., PhyR) activation by phosphorylation (Fig. 6).

MATERIALS AND METHODS

***nepR* translation start assay.** To measure translation from each the three putative *nepR* start codons, we constructed translational fusions of each potential start site to *lacZ* in the reporter plasmid pPR9TT (cut with AvrII-PstI). Primers used to amplify these different alleles are listed in Table S1 in the supplemental material. All plasmids with the corresponding inserts were sequence confirmed. Purified reporter plasmids were transformed into electrocompetent *Caulobacter crescentus* CB15. Single colonies of these reporter strains were used to inoculate 3 ml of peptone-yeast extract (PYE) medium supplemented with 2 μg/ml chloramphenicol (Chlor). Cultures were incubated overnight at 30°C and shaken at 220 rpm. Overnight cultures were diluted back in fresh PYE medium (with 2 μg/ml Chlor) at an optical density at 660 nm (OD$_{660}$) of ~0.05. At an OD$_{660}$ of ~0.2 (30°C/220 rpm), β-galactosidase activity was measured in triplicate as previously described (30). For strain information, see Table S2.

TABLE 2 Calculated phospho-PhyR (PhyR~P) half-life in the presence of buffer, MBP, MBP-NepR$_{FL}$ or MBP-NepR$_{SV}$[a]

Protein	PhyR~P half-life (h)
PhyR~P + buffer	45.7 ± 6.8
PhyR~P + MBP	44.6 ± 8.5
PhyR~P + MBP-NepR$_{FL}$	49.9 ± 2.2
PhyR~P + MBP-NepR$_{SV}$	47.8 ± 3.8

[a] Values presented are the averages of results from three independent experiments ± standard deviations.

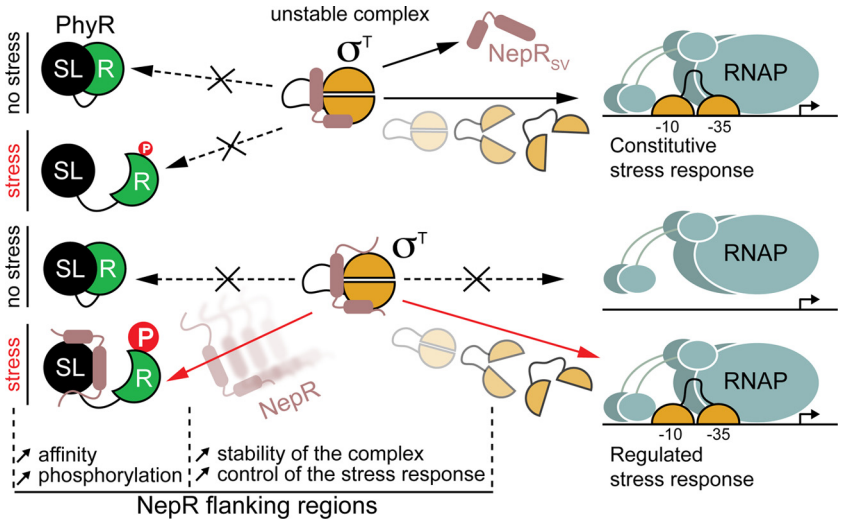

FIG 6 NepR anti-σ function requires its unconserved, disordered termini. A $NepR_{SV}$ allele missing the termini does not bind phospho-PhyR and forms a less stably folded complex with σ^T. Notably, phosphorylation of PhyR *in vitro* is strongly enhanced by addition of NepR, suggesting an additional layer of GSR regulation in which direct NepR interaction can influence activation of PhyR as an anti-anti-σ factor.

Bacterial two-hybrid protein interaction assay. To assay interaction between NepR fragments [FL, SV, SV + linker, SC2, SC3, ΔFR1, ΔFR2, and poly-A] and PhyR (wild type [WT], D192A, or SL) or σ^T inside bacterial cells, we used a bacterial two-hybrid system (19). The different *nepR* alleles were cloned into the pUT18c vector (digested with BamHI-EcoRI), which generated C-terminal fusions to the T18 fragment of adenylate cyclase. *phyR*, *phyR-SL*, and *sigT* were cloned into the pKT25 vector (digested with XbaI-KpnI). As a control the "reverse experiment" was also performed, and the different *nepR* alleles (FL and SV) were cloned into the pKT25 vector (digested with XbaI-KpnI); *phyR*, *phyR-SL*, and *sigT* were cloned into pUT18c (digested with BamHI-EcoRI and KpnI-EcoRI, respectively). The $nepR_{SV}$ + linker was synthesized as a GeneBlock (IDT). Primers used for PCRs are listed in Table S1 in the supplemental material; all plasmids were sequence confirmed. pUT18c and pKT25 combinations were transformed into electrocompetent *E. coli* reporter strain BTH101 and plated on LB agar supplemented with ampicillin (Amp; 100 μg/ml), kanamycin (Kan; 50 μg/ml), isopropyl-β-D-thiogalactopyranoside (IPTG; 1 mM), and 5-bromo-4-chloro-3-indolyl-β-D-galactopyranoside (X-Gal; 40 μg/ml). Control strains transformed with pKT25-Zip + pUT18c-Zip, pKT25 + pUT18c, pKT25-(*phyR/phyR-SL/sigT*) + pUT18c, pKT25 + pUT18c-*nepR*(alleles), pKT25-*nepR*(alleles) + pUT18c, and pKT25 + pUT18c-(*phyR/phyR-SL/sigT*) are shown in Fig. 2 and in Fig. S3 in the supplemental material. For further strain information, see Table S2.

After 48 h at 30°C, single colonies were used to inoculate 3 ml LB broth supplemented with Amp (100 μg/ml), Kan (50 μg/ml), and IPTG (1 mM); these cultures were grown overnight (30°C, 220 rpm) and used to inoculate 3 ml of fresh LB (Amp-Kan-IPTG) at an OD_{600} of ~0.05. Once the OD_{600} of these diluted cultures reached 0.5, β-galactosidase activity was measured in triplicate as previously described (30).

Western blot analysis. Western blotting assays were carried out using antiserum against the T18 fragment fused to various NepR alleles. Briefly, overnight cultures of the BTH101 strains transformed with different versions of pUT18c and pKT25 plasmids were used to inoculate 350 ml of LB medium supplemented with Amp (100 μg/ml), Kan (50 μg/ml), and IPTG (1 mM). Cultures were grown at 30°C and 220 rpm to an OD_{600} of ~0.8. Cells were then harvested by centrifugation at 8,000 rpm for 20 min at 4°C and resuspended in 10 ml of 25 mM Tris-HCl (pH 7.6), 125 mM NaCl buffer supplemented with phenylmethylsulfonyl fluoride (PMSF; 1 μl/ml), 1 mM EDTA, and 0.1% (vol/vol) Triton X-100. Cells were disrupted by three passages through a French pressure cell and clarified by centrifugation at 14,000 rpm for 20 min at 4°C.

Soluble fractions were transferred to new tubes, and total protein concentration was estimated using a commercial bicinchoninic acid (BCA) protein assay kit (Pierce). Appropriate lysate dilutions were heated in 3× SDS loading buffer at 95°C for 5 min, and 20 μl of sample was loaded onto a 15% SDS-PAGE gel and run for 2 h at 200 V. Samples were transferred to a Millipore 0.45-μm polyvinylidene difluoride (PVDF) membrane (Millipore) using a Trans-Blot turbo transfer system (Bio-Rad). After transfer, the membrane was washed in Tris-buffered saline–Tween 20 (TBST) supplemented with 5% milk and blocked overnight in fresh milk solution. The membrane was then incubated with 10 ml of TBST, 5% milk with a 1:1,000 dilution of anti-T18 antibody (3D1; KeraFast) for 1 h at room temperature. After a 30-min wash with TBST, the membrane was incubated for 1 h in 10 ml TBST, 5% milk with a 1:5,000 dilution of HRP-conjugated anti-mouse–horseradish peroxidase (HRP; Thermo Scientific) secondary antibody. After a final 30-min wash in TBST, the Western blot was developed with SuperSignal West Femto chemiluminescent substrate (Thermo Fisher Scientific). To visualize the bands and quantify the total amount of protein loaded in the gel, we used the Bio-Rad ChemiDoc MP imaging system.

PhyR Western blotting assays were performed using the sample preparation and transfer protocols detailed above. For PhyR recognition, anti-PhyR antibodies derived against *Brucella abortus* PhyR (15) were used at a dilution of 1:5,000 in 10 ml TBST, 5% milk. For visualization, a 1:5,000 dilution of HRP-conjugated mouse secondary antibody was used.,

For dot blot analysis of hemagglutinin (HA)-tagged $NepR_{FL}$ and $NepR_{SV}$ in *Caulobacter*, HA nucleotide sequence was inserted in frame at the C or N terminus of the *nepR* alleles by PCR sewing and cloned into pMT806 (digested with NdeI-XhoI). After sequence confirmation, all plasmids were transformed into the electrocompetent *C. crescentus* CB15 Δ*nepR* Δ*sigT*/pMT464-*sigT* strain (see strain and primer information in Tables S1 and S2 in the supplemental material). Overnight cultures of CB15 Δ*nepR* Δ*sigT*/pMT464-*sigT*/pMT806, CB15 Δ*nepR* Δ*sigT*/pMT464-*sigT*/pMT806-*HA*-$nepR_{FL}$ or pMT806-$nepR_{FL}$-*HA*, and CB15 Δ*nepR* Δ*sigT*/pMT464-*sigT*/pMT806-*HA*-$nepR_{SV}$ or pMT806-$nepR_{SV}$-*HA* were grown to an OD_{660} of ~0.1 in 5 ml of PYE (25 μg/ml Kan plus 1 μg/ml Chlor) and induced with vanillate (0.5 mM) and xylose (0.15%) for 4 h. Cells were spun down and suspended in 3× SDS loading buffer to an OD_{660} of 100. Samples were boiled and then spotted onto a 0.2-μm PVDF (Millipore) membrane. After transfer, the membrane was washed in Tris-buffered saline–Tween 20 (TBST) supplemented with 5% milk and blocked overnight in fresh milk solution. The membrane was then incubated with 10 ml of TBST, 5% milk with a 1:2,000 dilution of HA

antibody (Thermo Scientific) for 1 h at room temperature. After a 30-min wash with TBST, the membrane was incubated for 1 h in 10 ml TBST, 5% milk with a 1:5,000 dilution of HRP-conjugated anti-mouse secondary antibody. After a final 30-min wash in TBST, the Western blot was developed with SuperSignal West Femto chemiluminescent substrate (Thermo Fisher Scientific). To visualize the spots and quantify them, we used the Bio-Rad ChemiDoc MP imaging system.

Construction of *C. crescentus* mutant strains. To delete the *nepR-sigT* operon from the *C. crescentus* chromosome, a *sacB* suicide plasmid, pNPTS138, carrying 500-nucleotide regions flanking the 5′ and 3′ ends of the *nepR-sigT* operon was built. Primers (carrying EcoRI-SalI restriction sites) used to construct the deletion allele by overlapping PCR are listed in Table S1 in the supplemental material. The *nepR-sigT* knockout plasmid was transformed into the electrocompetent *C. crescentus* CB15 wild-type strain, and cells containing the integrated knockout plasmid were selected on PYE agar supplemented with 5 μg/ml Kan. Sucrose counterselection for crossover recombination to yield the *nepR-sigT* deletion strain (Δ*nepR* Δ*sigT*) was performed as previously described (31, 32).

Plasmids pRKLac290-P_{sigU} (encoding Tet^r), pMT464-*sigT* (encoding Kan^r), pMT806-*nepR*$_{FL}$, and pMT806-*nepR*$_{SV}$ (encoding Cam^r) were transformed into the Δ*nepR* Δ*sigT* strain by electroporation. pMT464-*sigT* was used to induce expression of *sigT* from a xylose-inducible promoter (P_{xyl}); pMT806 (restriction sites NdeI-XhoI) (33) was used to generate constructs from which NepR$_{FL}$ and NepR$_{SV}$ could be expressed from a vanillate-inducible promoter (P_{van}). Primers used to build these constructs are listed in Table S1 in the supplemental material. pRKLac290-P_{sigU} and pMT464-*sigT* were purified from preexisting strains FC634 and FC2251, respectively (11). All plasmids were sequence verified. To control for plasmid effects, empty pMT464 and pMT806 plasmids were transformed when needed into wild-type *C. crescentus* CB15 (strain number FC19) and the Δ*nepR* Δ*sigT* strain.

Stress response transcription assays. It is known that transcription of *sigU* is upregulated by the general stress σ factor σ^T upon hyperosmotic or oxidative stress challenge (17). The plasmid pRKLac290-P_{sigU} (Tet^r) (11), which contains the *sigU* promoter transcriptionally fused to *lacZ*, was conjugated into the different *C. crescentus* backgrounds (in some cases carrying pMT464 and pMT806 P_{xyl} and P_{van} constructs) to assay σ^T-dependent transcription. All *C. crescentus* strains were grown in PYE (2 μg/ml Chlor, 5 μg/ml Kan, and 1 μg/ml Tet) and diluted to a starting OD_{660} of 0.05 (30°C, 220 rpm). Cells were hyperosmotically stressed by adding 150 mM sucrose to the culture medium at the beginning of the experiment. Induced expression of *phyR* and *nepR* alleles from the *xyl* and *van* promoters was carried out by adding 0.15% xylose or 0.5 mM vanillate to the culture medium. β-Galactosidase activities were measured at an OD_{660} of ~0.25 in triplicate as previously described (34).

Recombinant protein expression strain construction. Previously published *E. coli* Rosetta (DE3)pLysS strains were used for the heterologous overexpression of *Caulobacter* His-PhyR, His-PhyR-SL, MBP-NepR$_{FL}$, and MBP (5); these strains are listed in Table S2 in the supplemental material.

Primers used to amplify and build the other expression strains are listed in Table S1 in the supplemental material. For expression of MBP-NepR$_{SV}$, the *nepR*$_{SV}$ PCR product was cloned into pMalc2g (Amp^r) digested with EcoRI-HindIII. For expression of His-PhyR$_{D192A}$, pKT25-PhyR$_{D192A}$ was used as a PCR template and the corresponding insert was cloned into pET28c (Kan^r) digested with NdeI-EcoRI. For coexpression of σ^T with NepR$_{FL}$ or NepR$_{SV}$, the different inserts were cloned into pETDuet-1 (Amp^r). The His tag was carried by σ^T, the corresponding insert was cloned at the first position of pETDuet-1, using EcoRI-NotI as restriction sites. The different NepR alleles (NepR$_{FL}$, NepR$_{SV}$, MBP-NepR$_{FL}$, and MBP-NepR$_{SV}$) and MBP were then inserted at the second position using the NdeI-KpnI restriction sites. To amplify by PCR the MBP-tagged NepR alleles, we used the pMalc2g-NepR FL and SV as the templates. After sequence confirmation, all the different expression plasmids were transformed into the chemically competent *E. coli* Rosetta (DE3)pLysS strain (see strain information in Tables S1 and S2).

Protein expression and purification. A 100-ml overnight LB culture was used to inoculate 1 liter of LB medium supplemented with the appropriate antibiotics. The different versions of His-PhyR, MBP-NepR proteins, and His-σ^T/NepR complexes were induced at an OD_{600} of 0.8 (37°C, 220 rpm) by adding 1 mM IPTG. After 5 h of induction, cells were harvested by centrifugation at 8,000 rpm for 20 min at 4°C. Cell pellets were resuspended in 10 mM Tris-HCl (pH 7.4), 150 mM NaCl, 10 mM imidazole buffer supplemented with 5 μg/ml of DNase I and 80 μg/ml of PMSF and disrupted by three passages in a French pressure cell. The resulting cell lysate was clarified by centrifugation at 14,000 rpm for 20 min at 4°C.

Purification of His-tagged proteins was performed using nickel affinity chromatography (nitrilotriacetic acid [NTA] resin; GE Healthcare). After the samples were bound to the column, three washing steps were performed using 10 mM, 30 mM, and 75 mM imidazole Tris-NaCl buffer followed by elution with 500 mM imidazole Tris-NaCl buffer. For purification of MBP-tagged fusion proteins, an amylose resin column (New England Biolabs) was first equilibrated with 10 mM Tris-HCl (pH 7.4) and 150 mM NaCl buffer. The clarified cell lysate was loaded and washed 5 times with 3 column volumes of equilibration buffer. Protein was eluted with equilibration buffer supplemented with 50 mM maltose. All purification steps were carried out at 4°C. In certain cases, after affinity purification, protein samples were further purified by size exclusion chromatography. Concentrated samples (300 μl at 10 mg/ml) were injected on a GE Healthcare Superdex 200 10/300 GL column (flow rate, 0.5 ml/min); fractions of 500 μl were collected during the run. Protein standards (blue dextran [2,000 kDa; void, ~11.9 ml], aldolase [158 kDa; elution, ~17.3 ml], conalbumin [75 kDa; elution, ~18.6 ml], and ovalbumin [43 kDa; elution, ~19.2 ml]) were injected in the column, and the corresponding calibration curve was use for size estimation of the different complexes.

Protein purity was assessed by resolving the different samples on 14% or 16% SDS-PAGE gels stained with Coomassie blue. All purified proteins were dialyzed overnight at 4°C against 2 liters of dialysis buffer (10 mM Tris-HCl [pH 7.4], 150 mM NaCl). Concentrations were assessed at 280 nm using a NanoDrop 1000 spectrophotometer (Thermo Scientific). When necessary, purified proteins were concentrated using a centrifugal filter (3-kDa molecular mass cutoff; Amicon-Millipore).

SPR binding assays. The kinetics of PhyR (or PhyR-SL) binding to MBP-NepR$_{FL}$ and MBP-NepR$_{SV}$ were measured by surface plasmon resonance (SPR) using a ProteOn XPR 6-channel instrument (Bio-Rad) at room temperature (~25°C). A 25-amino-acid linker between the MBP tag and the different versions of NepR was used to ensure minimal steric clash between MBP and the PhyR substrates. Purified His-PhyR and His-PhyR-SL proteins were diluted to 125 nM (~60 response units) and 200 nM (~40 response units), respectively, and loaded onto an HTG Bio-Rad sensor chip for 1 min (30 μl/min). MBP-NepR$_{FL}$ and MBP-NepR$_{SV}$ at concentrations ranging from 62.5 nM to 1 μM were injected onto the SPR chip preloaded with the different His-PhyR variants for 2 min (30 μl/min). Interactions between MBP-NepR (FL or SV) and His-PhyR or His-PhyR-SL protein were assayed under phosphorylating conditions (using 50 mM Tris-HCl [pH 7.4], 150 mM NaCl, 5 mM $MgCl_2$, 5 mM acetyl phosphate, and 0.05% Tween 20) and nonphosphorylating conditions (50 mM Tris-HCl [pH 7.4], 150 mM NaCl, 5 mM $MgCl_2$, and 0.05% Tween 20), respectively. All protein dilutions were carried out in the buffer condition being tested. As a control, we used the MBP tag alone, which was previously shown to not interact with His-PhyR or His-PhyR-SL proteins, using the same protocol as described above (5) (see Fig. S5 in the supplemental material). PhyR~P/NepR$_{FL}$, PhyR-SL/NepR$_{FL}$, and PhyR-SL/NepR$_{SV}$ raw binding data were analyzed in the ProteOn software suite using kinetic-Langmuir with drift analysis option. All SPR assays were conducted in triplicate.

Circular dichroism thermal denaturation measurements. The thermal denaturation profile of the different σ^T/NepR complexes was assayed using a Jasco J-1500 circular dichroism spectrometer. After dialysis in Tris-NaCl buffer (10 mM Tris-HCl [pH 7.4], 100 mM NaCl), 300 μl of protein purified by nickel affinity chromatography and size exclusion chromatography was loaded in a 1.0-mm quartz cuvette. Protein spectra were assayed at a 20 μM concentration. To ensure that all samples were correctly folded, we first acquired a full, buffer-subtracted CD spectrum (260 to 180 nm) for each sample at 26°C. For the thermal denaturation assay, temperature was gradually increased from 26°C to 74°C (2°C/min ramp). As the σ^T/NepR complex is all α-helical, we measured the loss of CD intensity at 222 nm. The corresponding melting curve (i.e., loss of signal at CD_{222nm}) was normalized, plotted. and fitted. Melt measurements on all samples were performed four times using independent protein preparations.

***In vitro* phosphorylation assays.** His-PhyR, His-$PhyR_{D192A}$, MBP-$NepR_{FL}$, MBP-$NepR_{SV}$, and MBP were purified as described above. *In vitro* phosphorylation of PhyR using radiolabeled acetyl phosphate ([^{32}P]AcP) was performed as previously described (35, 36). Briefly, for a 300-μl AcP reaction mixture, PhyR (10 μM final concentration) was incubated with 0.1 U of acetate kinase (Sigma-Aldrich), 5 μl [^{32}P]ATP (6,000 Ci/mmol), and 150 μl of 2× AcP buffer (25 mM Tris-HCl [pH 8.0], 60 mM potassium acetate, 10 mM $MgCl_2$). When indicated, reaction mixtures were supplemented with 10 μM concentrations of 3- to 7-day-old preparations of MBP, MBP-$NepR_{FL}$, or MBP-$NepR_{SV}$. For measurements of *in vitro* phosphorylation rates, samples were stopped by addition to equal-volume SDS loading buffer at the indicated time points and stored at −20°C until gels were run. All gels were exposed for equivalent periods of time on the same phosphor screen and imaged on a Bio-Rad FX imager. For each condition, the percentage of phosphorylated PhyR was calculated using ImageJ; the PhyR~P/MBP-$NepR_{FL}$ final time point was considered 100%. For calculating PhyR~P phosphoryl half-life, unincorporated [^{32}P]AcP was first removed by running the sample over a Zeba 7,000-molecular-weight-cutoff (MWCO) desalting column that was equilibrated in dialysis buffer. All samples were separated on Bio-Rad Any kD TGX gels before exposure to a phosphor screen (Molecular Dynamics) and subsequent visualization on a Bio-Rad FX imager. Gel images were analyzed using ImageJ (37). All experiments were performed in triplicate.

SUPPLEMENTAL MATERIAL

Supplemental material for this article may be found at http://mbio.asm.org/lookup/suppl/doi:10.1128/mBio.00910-15/-/DCSupplemental.

Figure S1, PDF file, 0.8 MB.
Figure S2, PDF file, 0.4 MB.
Figure S3, PDF file, 0.7 MB.
Figure S4, PDF file, 1 MB.
Figure S5, PDF file, 2.3 MB.
Figure S6, PDF file, 0.7 MB.
Table S1, PDF file, 0.1 MB.
Table S2, PDF file, 0.1 MB.

ACKNOWLEDGMENTS

S.C. acknowledges support for this study from National Institutes of Health award R01GM087353. J.W.W. is supported by National Institutes of Health NRSA F32GM109661.

We thank Elena Solomaha (University of Chicago Biophysics Core) for assistance with binding studies and Aretha Fiebig for helpful discussions.

REFERENCES

1. **Francez-Charlot A, Frunzke J, Reichen C, Ebneter JZ, Gourion B, Vorholt JA.** 2009. Sigma factor mimicry involved in regulation of general stress response. Proc Natl Acad Sci U S A **106:**3467–3472. http://dx.doi.org/10.1073/pnas.0810291106.
2. **Staroń A, Sofia HJ, Dietrich S, Ulrich LE, Liesegang H, Mascher T.** 2009. The third pillar of bacterial signal transduction: classification of the extracytoplasmic function (ECF) sigma factor protein family. Mol Microbiol **74:**557–581. http://dx.doi.org/10.1111/j.1365-2958.2009.06870.x.
3. **Francez-Charlot A, Kaczmarczyk A, Fischer HM, Vorholt JA.** 2015. The general stress response in alphaproteobacteria. Trends Microbiol **23:**164–171. http://dx.doi.org/10.1016/j.tim.2014.12.006.
4. **Campagne S, Damberger FF, Kaczmarczyk A, Francez-Charlot A, Allain FH, Vorholt JA.** 2012. Structural basis for sigma factor mimicry in the general stress response of alphaproteobacteria. Proc Natl Acad Sci U S A **109:**E1405–E1414. http://dx.doi.org/10.1073/pnas.1117003109.
5. **Herrou J, Rotskoff G, Luo Y, Roux B, Crosson S.** 2012. Structural basis of a protein partner switch that regulates the general stress response of alpha-proteobacteria. Proc Natl Acad Sci U S A **109:**E1415–E1423. http://dx.doi.org/10.1073/pnas.1116887109.
6. **Abromaitis S, Koehler JE.** 2013. The *Bartonella quintana* extracytoplasmic function sigma factor RpoE has a role in bacterial adaptation to the arthropod vector environment. J Bacteriol **195:**2662–2674. http://dx.doi.org/10.1128/JB.01972-12.
7. **Bastiat B, Sauviac L, Bruand C.** 2010. Dual control of *Sinorhizobium meliloti* RpoE2 sigma factor activity by two PhyR-type two-component response regulators. J Bacteriol **192:**2255–2265. http://dx.doi.org/10.1128/JB.01666-09.
8. **Correa F, Ko WH, Ocasio V, Bogomolni RA, Gardner KH.** 2013. Blue light regulated two-component systems: enzymatic and functional analyses of light-oxygen-voltage (LOV)-histidine kinases and downstream response regulators. Biochemistry **52:**4656–4666. http://dx.doi.org/10.1021/bi400617y.
9. **Gourion B, Francez-Charlot A, Vorholt JA.** 2008. PhyR is involved in the general stress response of *Methylobacterium extorquens* AM1. J Bacteriol **190:**1027–1035. http://dx.doi.org/10.1128/JB.01483-07.
10. **Gourion B, Sulser S, Frunzke J, Francez-Charlot A, Stiefel P, Pessi G, Vorholt JA, Fischer HM.** 2009. The PhyR-sigma(EcfG) signalling cascade is involved in stress response and symbiotic efficiency in *Bradyrhizobium japonicum*. Mol Microbiol **73:**291–305. http://dx.doi.org/10.1111/j.1365-2958.2009.06769.x.
11. **Herrou J, Foreman R, Fiebig A, Crosson S.** 2010. A structural model of anti-anti-sigma inhibition by a two-component receiver domain: the PhyR stress response regulator. Mol Microbiol **78:**290–304. http://dx.doi.org/10.1111/j.1365-2958.2010.07323.x.
12. **Iguchi H, Sato I, Yurimoto H, Sakai Y.** 2013. Stress resistance and C1 metabolism involved in plant colonization of a methanotroph *Methylosinus* sp. B4S. Arch Microbiol **195:**717–726. http://dx.doi.org/10.1007/s00203-013-0922-6.
13. **Jans A, Vercruysse M, Gao S, Engelen K, Lambrichts I, Fauvart M, Michiels J.** 2013. Canonical and non-canonical EcfG sigma factors control the general stress response in *Rhizobium etli*. Microbiologyopen **2:**976–987. http://dx.doi.org/10.1002/mbo3.137.
14. **Kaczmarczyk A, Campagne S, Danza F, Metzger LC, Vorholt JA, Francez-Charlot A.** 2011. Role of *Sphingomonas* sp. strain fr1 PhyR-NepR-sigmaEcfG cascade in general stress response and identification of a negative regulator of PhyR. J Bacteriol **193:**6629–6638. http://dx.doi.org/10.1128/JB.06006-11.
15. **Kim HS, Caswell CC, Foreman R, Roop RM, II, Crosson S.** 2013. The *Brucella abortus* general stress response system regulates chronic mammalian infection and is controlled by phosphorylation and proteolysis. J Biol Chem **288:**13906–13916. http://dx.doi.org/10.1074/jbc.M113.459305.
16. **Lourenço RF, Kohler C, Gomes SL.** 2011. A two-component system, an anti-sigma factor and two paralogous ECF sigma factors are involved in the control of general stress response in *Caulobacter crescentus*. Mol Microbiol **80:**1598–1612. http://dx.doi.org/10.1111/j.1365-2958.2011.07668.x.
17. **Alvarez-Martinez CE, Lourenço RF, Baldini RL, Laub MT, Gomes SL.** 2007. The ECF sigma factor sigma(T) is involved in osmotic and oxidative stress responses in *Caulobacter crescentus*. Mol Microbiol **66:**1240–1255. http://dx.doi.org/10.1111/j.1365-2958.2007.06005.x.
18. **Schrader JM, Zhou B, Li GW, Lasker K, Childers WS, Williams B, Long T, Crosson S, McAdams HH, Weissman JS, Shapiro L.** 2014. The coding and noncoding architecture of the *Caulobacter crescentus* genome. PLoS Genet **10:**e1004463. http://dx.doi.org/10.1371/journal.pgen.1004463.
19. **Karimova G, Pidoux J, Ullmann A, Ladant D.** 1998. A bacterial two-hybrid system based on a reconstituted signal transduction pathway. Proc Natl Acad Sci U S A **95:**5752–5756. http://dx.doi.org/10.1073/pnas.95.10.5752.

20. **Wolfe AJ**. 2005. The acetate switch. Microbiol Mol Biol Rev **69:**12–50. http://dx.doi.org/10.1128/MMBR.69.1.12-50.2005.
21. **Xue B, Dunbrack RL, Williams RW, Dunker AK, Uversky VN**. 2010. PONDR-FIT: a meta-predictor of intrinsically disordered amino acids. Biochim Biophys Acta **1804:**996–1010. http://dx.doi.org/10.1016/j.bbapap.2010.01.011.
22. **Cheng J, Sweredoski MJ, Baldi P**. 2005. Accurate prediction of protein disordered regions by mining protein structure data. Data Min Knowl Discov **11:**213–222. http://dx.doi.org/10.1007/s10618-005-0001-y.
23. **Sauviac L, Philippe H, Phok K, Bruand C**. 2007. An extracytoplasmic function sigma factor acts as a general stress response regulator in *Sinorhizobium meliloti*. J Bacteriol **189:**4204–4216. http://dx.doi.org/10.1128/JB.00175-07.
24. **Campagne S, Allain FH, Vorholt JA**. 2015. Extra cytoplasmic function sigma factors, recent structural insights into promoter recognition and regulation. Curr Opin Struct Biol **30:**71–78. http://dx.doi.org/10.1016/j.sbi.2015.01.006.
25. **Ganguly A, Chatterji D**. 2012. A comparative kinetic and thermodynamic perspective of the sigma-competition model in Escherichia coli. Biophys J **103:**1325–1333. http://dx.doi.org/10.1016/j.bpj.2012.08.013.
26. **Schuster M, Silversmith RE, Bourret RB**. 2001. Conformational coupling in the chemotaxis response regulator CheY. Proc Natl Acad Sci U S A **98:**6003–6008. http://dx.doi.org/10.1073/pnas.101571298.
27. **Barbieri CM, Mack TR, Robinson VL, Miller MT, Stock AM**. 2010. Regulation of response regulator autophosphorylation through interdomain contacts. J Biol Chem **285:**32325–32335. http://dx.doi.org/10.1074/jbc.M110.157164.
28. **Kaczmarczyk A, Hochstrasser R, Vorholt JA, Francez-Charlot A**. 2014. Complex two-component signaling regulates the general stress response in alphaproteobacteria. Proc Natl Acad Sci U S A **111:**E5196–E5204. http://dx.doi.org/10.1073/pnas.1410095111.
29. **McCleary WR, Stock JB**. 1994. Acetyl phosphate and the activation of two-component response regulators. J Biol Chem **269:**31567–31572.
30. **Griffith KL, Wolf RE, Jr.** 2002. Measuring beta-galactosidase activity in bacteria: cell growth, permeabilization, and enzyme assays in 96-well arrays. Biochem Biophys Res Commun **290:**397–402. http://dx.doi.org/10.1006/bbrc.2001.6152.
31. **Fiebig A, Castro Rojas CM, Siegal-Gaskins D, Crosson S**. 2010. Interaction specificity, toxicity and regulation of a paralogous set of ParE/RelE-family toxin-antitoxin systems. Mol Microbiol **77:**236–251. http://dx.doi.org/10.1111/j.1365-2958.2010.07207.x.
32. **Ried JL, Collmer A**. 1987. An nptI-sacB-sacR cartridge for constructing directed, unmarked mutations in gram-negative bacteria by marker exchange-eviction mutagenesis. Gene **57:**239–246. http://dx.doi.org/10.1016/0378-1119(87)90127-2.
33. **Thanbichler M, Iniesta AA, Shapiro L**. 2007. A comprehensive set of plasmids for vanillate- and xylose-inducible gene expression in *Caulobacter crescentus*. Nucleic Acids Res **35:**e137. http://dx.doi.org/10.1093/nar/gkm818.
34. **Miller JH**. 1972. Experiments in molecular genetics, p 352–355. CSHL Press, Cold Spring Harbor, NY.
35. **Willett JW, Kirby JR**. 2012. Genetic and biochemical dissection of a HisKA domain identifies residues required exclusively for kinase and phosphatase activities. PLoS Genet **8:**e1003084. http://dx.doi.org/10.1371/journal.pgen.1003084.
36. **Willett JW, Tiwari N, Müller S, Hummels KR, Houtman JC, Fuentes EJ, Kirby JR**. 2013. Specificity residues determine binding affinity for two-component signal transduction systems. mBio **4**(6):e00420-13. http://dx.doi.org/10.1128/mBio.00420-13.
37. **Schneider CA, Rasband WS, Eliceiri KW**. 2012. NIH image to ImageJ: 25 years of image analysis. Nat Methods **9:**671–675. http://dx.doi.org/10.1038/nmeth.2089.